STEM CELLS TRANSLATIONAL MEDICINE®

TISSUE-SPECIFIC PROGENITOR AND STEM CELLS

MSC-Seeded Biomimetic Scaffolds as a Factory of Soluble RANKL in Rankl-Deficient Osteopetrosis

CIRO MENALE,[a,b] ELISABETTA CAMPODONI,[c] ELEONORA PALAGANO,[b,d] STEFANO MANTERO,[a,b] MARCO ERRENI,[b] ANTONIO INFORZATO,[b,d] ELENA FONTANA,[a,b] FRANCESCA SCHENA,[e] ROB VAN'T HOF,[f] MONICA SANDRI,[c] ANNA TAMPIERI,[c] ANNA VILLA,[a,b] CRISTINA SOBACCHI [a,b]

Key Words. MSC • RANKL • cell therapy • gene therapy • biomimetic scaffold • Osteopetrosis

[a]CNR-IRGB, Milan Unit, Milan, Italy; [b]Humanitas Clinical and Research Institute, Rozzano, Italy; [c]CNR-ISTEC, Faenza, Italy; [d]Department of Medical Biotechnologies and Translational Medicine, University of Milan, Milan, Italy; [e]Clinica Pediatrica e Reumatologia, UOSD Centro Malattie Autoinfiammatorie e Immunodeficienze, Genoa, Italy; [f]Bone Research Group, Institute of Ageing & Chronic Disease, University of Liverpool, Liverpool, UK

Cristina Sobacchi, Humanitas Clinical and Research Institute, via Manzoni 113, 20089 Rozzano, Italy. Telephone: 39 02 82245153; Fax: 39 02 82245290; e-mail: cristina.sobacchi@humanitasresearch.it

Received 11 April 2018; revised 9 July 2018; accepted for publication 11 July 2018.

http://dx.doi.org/10.1002/sctm.18-0085

ABSTRACT

Biomimetic scaffolds are extremely versatile in terms of chemical composition and physical properties, which can be defined to accomplish specific applications. One property that can be added is the production/release of bioactive soluble factors, either directly from the biomaterial, or from cells embedded within the biomaterial. We reasoned that pursuing this strategy would be appropriate to setup a cell-based therapy for RANKL-deficient Autosomal Recessive Osteopetrosis, a very rare skeletal genetic disease in which lack of the essential osteoclastogenic factor RANKL impedes osteoclast formation. The exogenously administered RANKL cytokine is effective in achieving osteoclast formation and function in vitro and in vivo, thus, we produced murine *Rankl*$^{-/-}$ MSCs overexpressing human soluble RANKL (hsRL) following lentiviral transduction (LVhsRL). Here, we described a three-dimensional (3D) culture system based on a Magnesium-doped hydroxyapatite/collagen I (MgHA/Col) biocompatible scaffold closely reproducing bone physicochemical properties. MgHA/Col-seeded murine MSCs showed improved properties, as compared to two-dimensional (2D) culture, in terms of proliferation and hsRL production, with respect to LVhsRL-transduced cells. When implanted subcutaneously in *Rankl*$^{-/-}$ mice, these cell constructs were well tolerated, colonized by host cells, and intensely vascularized. Of note, in the bone of *Rankl*$^{-/-}$ mice that carried scaffolds with either WT or LVhsRL-transduced *Rankl*$^{-/-}$ MSCs, we specifically observed formation of TRAP^{+} cells, likely due to sRL released from the scaffolds into circulation. Thus, our strategy proved to have the potential to elicit an effect on the bone; further work is required to maximize these benefits and achieve improvements of the skeletal pathology in the treated *Rankl*$^{-/-}$ mice. STEM CELLS TRANSLATIONAL MEDICINE *2018*

SIGNIFICANCE STATEMENT

RANKL-deficient Autosomal Recessive Osteopetrosis is a very rare skeletal genetic disease in which lack of the essential osteoclastogenic factor RANKL impedes osteoclast formation and bone resorption, and causes extremely high bone density and secondary hematological and neurological defects. At present, there is no cure for this disease. Here we demonstrated that RANKL-releasing MSC-seeded biomimetic constructs implanted subcutaneously in *Rankl*$^{-/-}$ mice served as a source of the missing cytokine and restored the formation of TRAP^{+} cells in bone, thus providing proof of principle of the capacity of this approach to support cell differentiation towards the osteoclast lineage in vivo. Implementation of the experimental setting by means of recent biotechnological tools will increase the effectiveness of this strategy on the bone compartment.

INTRODUCTION

Over the last 15 years a great variety of biomimetic scaffolds, rationally designed devices with specific physicochemical properties, conceived to be seeded with cells, and used in vivo to elicit or replace a missing function that cannot be promptly restored by cells only, have been developed [1]. In the bone field, biomimetic scaffolds are exploited for their osteoinductive and osteoconductive properties; in basic studies, they constitute a tool for evaluating osteogenic potential of Mesenchymal Stromal Cells (MSCs) from different tissues in ectopic bone formation assays [2]. In translational studies, a range of strategies for tissue engineering have been implemented; in the majority of cases, bone-like scaffolds support and induce bone regeneration to replace areas of bone loss in large defects or at load-bearing sites [3]. Biomaterials may also serve as a source of bioactive soluble factors; these may be either incorporated in the scaffold during its production and released from there in specific environmental conditions, or secreted

by cells seeded on these three-dimensional (3D) structures [4, 5].

Our work intended to evaluate this latter application in the context of Receptor Activator of Nuclear Factor k B Ligand-deficient Autosomal Recessive Osteopetrosis (RANKL-ARO), a rare genetic skeletal disease in which lack of production of the essential osteoclastogenic molecule RANKL by cells of the stromal compartment in bone hinders osteoclast formation and bone resorption. This leads to extremely high bone density and secondary hematological and neurological defects, which further compromise the clinical picture, hence threatening the patients' survival [6]. At variance with other known forms of ARO, in which the defect is cell autonomous and early Hematopoietic Stem Cell Transplantation (HSCT) is an effective cure, in RANKL-ARO the osteoclast defect is not cell-autonomous, thus it cannot be rescued by HSCT [7, 8]. Thus, defining a cure for RANKL-ARO is currently an unmet medical need, whose solution is unfairly complicated owing to the extreme rarity of these patients.

Thanks to the availability of a mouse model (Rankl knockout, *Rankl*$^{-/-}$) closely resembling the human disease, and to the biological activity in vivo of soluble RANKL, two different targeted therapeutic approaches have been evaluated at a preclinical level: a pharmacological and a cell-based one [9, 10]. The former consisted of the exogenous administration of soluble recombinant RANKL to *Rankl*$^{-/-}$ mice; in our work, we evaluated different treatment schedules and identified a specific protocol able to correct the bone pathology [9]. As an alternative way to provide the defective cytokine, Cappariello and colleagues assembled diffusion chambers containing osteoblasts seeded on a matrix metalloprotease 14 (MMP14)-functionalized scaffold to facilitate RANKL shedding from the cell membrane, and implanted them in vivo [10]. This strategy overcame the major limitation of the pharmacological approach, that is, the requirement for high quality (Good Manufacturing Practice, GMP-level) recombinant RANKL for a thorough preclinical study; however, it required invasive surgery to obtain sufficient RANKL release as compared to in vivo cytokine administration.

Based on the nature of the defect in RANKL-ARO, here we devised an approach based on Mesenchymal Stromal Cells (MSCs), multipotent stromal cells characterized by in vitro plastic adherence, colony-forming capacity, expression of a panel of surface molecules, and ability to differentiate at least toward the osteogenic, adipogenic, and chondrogenic lineages [11]. In regenerative medicine, they represent a valuable tool capable of restoring normal tissue function through the stimulation of repair mechanisms by the host's cells [12]. This mainly occurs via the production of a wide range of trophic factors, also comprised of the RANKL cytokine [3, 11, 13–15]. On this basis, MSCs are under evaluation for cell therapy of a range of disorders, which could be combined with gene delivery via viral vectors to elicit specific MSC properties [16].

Moreover, increasing evidence showed that MSC features are strictly dependent on environmental, physical, mechanical, and chemical characteristics, and this drove the engineering of biomimetic scaffolds artificially reproducing selected natural microenvironments [17].

Of note, we recently reported the generation of wild type (WT) and *Rankl*$^{-/-}$ murine MSC lines, and, in the latter, the restoration of RANKL production and osteogenic capacity by transduction with a lentiviral vector expressing human soluble RANKL [13]. Based on the close resemblance of RANKL-defective osteopetrosis in humans and mice, we envisage RANKL production might be similarly reestablished in patient-derived cells.

Overall, these data provided the rationale for our novel approach: we hypothesized that MSC-seeded scaffolds carrying either WT or transduced cells, might serve as a factory of soluble RANKL, and thus provide the cytokine in Rankl-deficient osteopetrosis to restore osteoclastogenesis. Here, we describe the establishment of murine MSC 3D cultures on a bone biomimetic scaffold and provide proof-of-principle that subcutaneous implantation of these scaffolds seeded with RANKL-expressing MSCs in *Rankl*$^{-/-}$ mice restores formation of TRAP^{+} cells, bona fide osteoclasts in the bone tissue.

Materials and Methods

Cell Culture

The Human Embryonic Kidney 293 T (HEK293T) cell line was purchased from ATCC and cultured in IMDM medium supplemented with 10% fetal bovine serum (FBS; both from GIBCO, Grand Island, NY), 1% penicillin/streptomycin and 1% glutamine (Lonza, Basel, Swizerland).

Bone marrow-derived mesenchymal stromal cells (MSCs) were isolated, cultured, and characterized as previously described from both WT and *Rankl*$^{-/-}$ mice [13]. Cells were kept in a humidified 5% CO_2 incubator at 37°C.

Lentiviral Transduction

The third-generation bidirectional lentiviral vectors (LVhsRL and mock) used for HEK293T and MSCs transduction have been already described [13]. Briefly, the IgK-chain leader secretion signal followed by the extracellular region of human RANKL (nucleotides 416-954, NM_003701) was inserted into the #1074.1071.hPGK.GFP.WPRE.mhCMV.dNGFR.SV40PA plasmid backbone (gift of Prof Luigi Naldini, San Raffaele Telethon Institute for Gene Therapy, Milan), according to standard protocols. The lentiviral vectors were produced following standard procedures and in accordance with institutional and national laws (notification n. MI/IC/IMP2/12-003).

The day before transduction, HEK293T cells were plated at a density of 10^4 cells/cm^2 in 6-well plate. Lentiviral transduction was performed in 1.0 ml culture medium at a multiplicity of infection (MOI) ranging from 1 to 100, in the presence of 8 μg/ml Polybrene (Sigma-Aldrich, Saint Louis, MO); untransduced cells were treated with Polybrene only as control. After 16 hours, the medium was replaced with fresh culture medium. Transduced cells expressing GFP were analyzed by flow cytometry (FACSCantoII, BD Bioscience, Eysins, Switzerland) to assess GFP fluorescence. HEK293T cell viability was evaluated through the dye exclusion test with Trypan blue and by MTT Test, following standard procedures. Two weeks after transduction, vector copy number (VCN) was determined by qPCR as previously described [18].

Rankl$^{-/-}$ MSCs were transduced with either LVhsRL or mock lentiviral vector at 20 MOI, as previously described, and maintained in MSC complete Mesencult medium (Stemcell Technologies, Vancouver, BC) [13].

RANKL Protein Analysis

Total protein extraction, gel electrophoresis, transfer, and visualization were performed according to standard Western blotting procedures. Briefly, cell lysis was done in RIPA buffer and

proteins were quantified using the DC Protein Assay Kit II (Biorad, Berkeley, CA) following the manufacturer's instructions, on a Synergy H4 instrument (BioTek Instruments, Inc., Winooski, VT). Twenty-five micrograms of protein extracts were separated on a 10% Sodium Dodecyl Sulfate Polyacrylamide Gel Electrophoresis (SDS-PAGE) and transferred to a nitrocellulose membrane. This was incubated with human RANKL monoclonal antibody (Alexis Corporation, Lausen, Switzerland), diluted 1:1,000 in 5% milk solution, for 2 hours at room temperature, then washed, probed with a secondary antibody conjugated with HRP and developed using the Immobilon Western kit (Millipore, Darmstadt, Germany). Images were acquired using the ChemiDoc MP Imaging System equipped with Image Lab Software (Biorad).

In Vitro Osteoclastogenesis and Resorption Assay

Conditioned culture medium (CM) from HEK293T cells transduced with either LVhsRL or the mock vector at 20 MOI underwent protein enrichment by Vivaspin column 10 MWCO (Sartorius, Goettingen, Germany) ultrafiltration according to the manufacturer's instructions, to obtain a ×50 concentrated CM with a final concentration of about 2 ng/ml hsRL.

In vitro osteoclastogenesis was induced in human PBMCs obtained from buffy coat of healthy donors by Ficoll separation or in murine WT and *Rankl*$^{-/-}$ murine splenocytes. Briefly, 4×10^5 cells/well were cultured in 96-well plate in αMEM medium (Sigma-Aldrich) supplemented with 10% FBS, 1% penicillin/streptomycin, and 1% glutamine in the presence of 25 ng/ml M-CSF, 5 ng/ml human TGFβ1 (both from Peprotech, London, UK), 1 μM Dexamethasone (Sigma-Aldrich) and with or without 100 μl/ml of either CM for 6 or 12 days (for murine and human cells, respectively). Mature osteoclasts were stained using the Tartrate Resistant Acid Phosphatase (TRAP) Kit (Sigma-Aldrich) following the manufacturer's instruction.

The same culture conditions were used to perform osteoclastogenesis on dentin discs (Immunodiagnostic Systems, Ltd., Scottsdale, AZ) to evaluate osteoclast resorption activity. After 3 weeks, dentin discs were rinsed with water, scraped to remove attached cells, stained with 1% toluidine blue solution for 3 minutes, and then washed with water to visualize resorption pits. Images were acquired on an EVOS XL Inverted Microscope (Thermo Fisher Scientific, Waltham, MA) for both TRAP$^+$ mature osteoclasts and toluidine blue stained dentin discs.

MgHA/Col Scaffold Synthesis

Equine tendon derived type I collagen, 1 wt.% in aqueous acetic buffered solution (pH 3.5), was purchased from Opocrin SpA (Modena, Italy). Phosphoric acid (H_3PO_4, 85 wt.%), calcium hydroxide ($Ca(OH)_2$, 95 wt.%), magnesium chloride hexahydrate ($MgCl_2{\cdot}6H_2O$, 99 wt.%), and 1,4-butanediol diglycidyl ether (BDDGE, 95 wt.%) were purchased from Sigma Aldrich. Phosphate buffer saline (PBS, pH 7.4) was supplied by EuroClone (Milan, Italy).

Briefly, 100 g of collagen gel were dissolved into a 0.04 M phosphoric acid solution, while 0.235 g of $MgCl_2{\cdot}6H_2O$ were added to a 0.07 M basic calcium suspension [19, 20]. The acid collagen slurry was added drop-wise into the basic calcium and magnesium suspension, leading to the formation of Mg-doped apatite nanocrystals uniformly distributed in the collagen matrix. After 2 hours at room temperature, the hybrid slurry was washed three times in distilled water and filtered to remove free ions. The cross-linking reaction was carried out in the presence of 20 ml of 1 g/L of BDDGE solution for 24 hours at room temperature, followed by 24 hours at 4°C [21, 22]. Afterward, the cross-linking solution was removed and the hybrid composite was washed three times with distilled water before pouring it into polystyrene 96-well plate. Porous 3D-hybrid scaffolds were obtained by freezing the collagen hydrogel at −40°C and drying it at 25°C (5 Pascal, LIO 3000 PLT, Milan, Italy) for 48 hours under a constant vacuum of 0.086 mbar. Finally, the scaffolds were sterilized by gamma-irradiation.

Scanning Electron Microscopy (SEM)

Specimens were mounted onto aluminum stubs using black carbon tapes and sputter coated with gold (Sputter Coater Q150TES, Laughton, UK). The specimen surface and scaffold microarchitecture were examined using high resolution SEM (FEI, Quanta 200, Cambridge, UK) under a pressure of 0.1 mTorr at an accelerating voltage of 7 or 10 kV.

Structural Characterization of MgHA/Col

The total porosity was calculated by the gravimetric (or density) method [23], according to the formula:

$$\text{total porosity}\,(\%) = 100 - \left(\frac{\rho}{\rho_{\text{theoretical}}} \times 100\right),$$

where ρ is the scaffold density determined with the equation:

$$\rho = \frac{W}{\pi \times \left(\frac{D}{2}\right)^2 \times H},$$

in which W is the weight, D is the diameter, and H is the height of the scaffold; and the theoretical density of the material is calculated from the theoretical density and weight fraction (X_A, X_B,…) of each reagent:

$$\rho_{\text{theoretical}} = \left(\rho_{\text{theoretical(A)}} \times X_A\right) + \left(\rho_{\text{theoretical(B)}} \times X_B\right).$$

The macropores volume percentage was calculated by the water squeezing method [24]. Briefly, the scaffold was equilibrated in deionized water for 1 hour and weighed (M_{swollen}), then squeezed to remove the water filling the pores and weighed again (M_{squeezed}). Macropores volume was calculated using the equation:

$$\text{Macropores volume percentage} = \frac{(M_{\text{swollen}} - M_{\text{squeezed}})}{M_{\text{swollen}}} \times 100.$$

All the values were expressed as the mean ± SEM (n = 3).

X-Ray Diffraction (XRD)

XRD patterns of the samples were recorded on a D8 Advance diffractometer (Bruker, Karlsruhe, Germany) equipped with a Lynx-eye position sensitive detector using Cu Kα radiation (I = 1.54178 Å) generated at 40 kV and 40 mA. XRD spectra were recorded in the 2θ range from 20° to 60° with a step size (2θ) of 0.02° and a counting time of 0.5 seconds.

Fourier Transform Infrared Spectroscopy (FTIR)

FTIR spectra were collected on a Nicolet 380 spectrometer (Thermo Fisher Scientific Inc.) with a resolution of 4 cm^{-1} by accumulation of 64 scans covering the 4,000 to 400 cm^{-1} range, using the KBr pellet method.

The pellets (13 mm ∅) were prepared by mixing 2 mg of ground sample with 100 mg of KBr in a mortar and pressing.

Inductively Coupled Plasma Optical Emission Spectrometry (ICP-OES)

Calcium, phosphate, and magnesium contents were determined by ICP-OES using a Liberty 200 spectrometer (Varian, Palo Alto, CA). Twenty milligram of sample were dissolved in 50 ml of a 1 wt.% HNO_3 solution prior to analysis.

Thermal Gravimetric Analysis (TGA)

The thermal properties and the ratio between collagen and MgHA in the hybrid sample were measured using a simultaneous thermal analyzer STA 449/C Jupiter (Netzsch, Germany). Simultaneous TGA was carried out on approximately 10 mg of sample placed in alumina crucibles, and then brought from room temperature to 1,200°C at a heating rate of 10°C/min under an airflow of 1 ml/min.

Swelling and Degradation Tests

The scaffolds were soaked in PBS, pH 7.2 in the presence of 0.1% (wt/vol) NaN_3 at 37°C. At specific time points, the samples were blotted with a piece of paper to remove surface droplets. The swelling ratio (*Qs*) was evaluated using the following equation:

$$Qs = \frac{W_s - W_d}{W_d},$$

where W_s is the weight of the swollen sample at a specific time point and W_d the initial weight of the dried sample.

In the degradation test, the scaffolds were soaked as above, then washed twice with milli-Q water, freeze-dried for 2 days and subsequently weighed. The degradation percentage (*D*) was evaluated using the following equation:

$$D(\%) = \frac{W_i - W_f}{W_i} \times 100,$$

where W_i is the initial weight of the dried sample and W_f the weight of the freeze-dried sample at a specific time point.

Standardization of MSC 3D Culture

Sterile MgHA/Col scaffolds were incubated overnight at 37°C in the MSC conventional culture medium. The day after, the scaffolds were placed in 48-well plate (1 scaffold/well). LVhsRL-MSCs with 5×10^5 were suspended in 30 µl of standard culture medium and dropped onto each scaffold. Cell attachment was allowed for 30 minutes at 37°C and 5% CO_2. Subsequently, 1 ml of cell culture medium was added to the cell-seeded 3D scaffold system to completely cover it. To evaluate cell morphology and behavior in 3D culture, we took advantage of GFP expression by transduced MSC and collagen autofluorescence. Cell-seeded scaffold systems were formalin fixed at 24, 48, and 72 hours after seeding and analyzed by confocal microscopy. Images were acquired with a laser-scanning confocal microscope (FluoView FV1000, Olympus Corp., Hamburg, Germany), with 405 and 488 nm wavelength laser excitation for collagen and GFP^+-MSC-transduced cell, respectively. The resulting fluorescence emissions were collected in a wavelength range from 425 to 475 nm (for collagen) and from 500 to 560 nm (for GFP^+ MSC-transduced cell). Images were acquired with a 10X UPLSAPO objective (Olympus); then, processing, analysis, 3D stack reconstruction and surface rendering were performed using Imaris ×64 7.6.5 software (Bitplane, Belfast, Ireland).

For the evaluation of MSC viability and human RANKL production over time, cell-seeded scaffolds were maintained up to 6 days and the medium changed every 2 days; conventional 2D culture of the same cells (5×10^5 cells in 6-well plate) was concomitantly performed as a control. For both 2D and 3D cultures, at days 2, 4, and 6, cell viability of WT, mock-transduced, and LVhsRL-transduced *Rankl*$^{-/-}$ MSCs was assessed through MTT assay. hsRL levels were measured after 3 days of culture by ELISA (PromoCell GmbH, Heidelberg, Germany) on the culture medium collected from LVhsRL-transduced *Rankl*$^{-/-}$ MSCs.

In Vivo Implantation

All mouse experimental procedures were performed in accordance with the Humanitas Institutional Animal Care and Use Committee and with international laws (authorization n.540/2017-PR). *Rankl*$^{+/-}$ mice were a kind gift of Prof. Yongwon Choi (University of Pennsylvania, Philadelphia, PA) [25]. The colony was maintained in heterozygosis in a specific pathogen-free facility; the litters were genotyped as described [25] and *Rankl*$^{-/-}$ mice were fed a soft diet after weaning. The study design comprised only *Rankl*$^{-/-}$ mice. In detail, 6 week old *Rankl*$^{-/-}$ mice (both males and females) were randomly divided in three groups: one was implanted with LVhsRL-transduced MSC-seeded scaffolds, another with mock-transduced MSC-seeded scaffolds and the last with WT MSC-seeded scaffold, as controls. In each group, mice were implanted with either 1 or 2 scaffolds, which were prepared following a different protocol: (a) 1 scaffold/mouse: seeding of 7×10^5 cells (WT MSC, or mock-transduced or LVhsRL-transduced MSC) and implantation after overnight culture at 37°C, 5% CO_2; (b) 2 scaffolds/mouse: seeding of 1.5×10^6 cells/scaffold (WT MSC, or mock-transduced or LVhsRL-transduced MSC), 3 days culture at 37°C, 5% CO_2 to allow cell penetration into the scaffold, and then implantation. In both protocols, the yield of cell seeding was calculated as a ratio between the amount of cells effectively attached to the scaffold (inferred as the difference between the number of seeded cells and that of cells left on the bottom of the well) and those initially seeded.

For the surgery, *Rankl*$^{-/-}$ mice underwent deep anesthesia (Ketamine/Xylazine) and were shaved on the back; then, under sterile conditions the skin was incised over the shoulders and a subcutaneous pouch was formed, in which the cell-seeded scaffold(s) was (were) inserted. The incision was sewn up with wire absorbable suture; then the mice were kept warm on a special hotplate and singly housed, when they had sufficiently recovered. After 8 weeks, mice were sacrificed by CO_2 asphyxiation; blood, scaffold systems, long bones, and soft tissues were collected for serological and histological evaluations.

Histological Analysis

The harvested scaffolds were fixed in 4% paraformaldehyde (PFA) and decalcified in ion exchange decal unit (Biocare Medical, Concord, CA), dehydrated and embedded in paraffin for hematoxylin and eosin (H&E) staining and for immunohistochemistry by using anti-GFP (Invitrogen Thermofisher; 1:200), anti-CD31 (R&D, Minneapolis, MN; 1:1,000), and anti-F4/80 (Biorad; 1:100) antibodies according to standard protocols.

Bones were fixed in 4% PFA for 48 hours, decalcified in 14% EDTA solution for 2 weeks and paraffin-embedded for TRAP staining with the Acid Phosphatase TRAP kit (Sigma-Aldrich). $TRAP^+$ cells were counted in at least two stained long bone sections per animal. Digital images were acquired with an Olympus XC50 camera mounted on a BX51 microscope (Olympus), and analyzed with CellF Imaging software (Soft Imaging System GmbH, Munster, Germany).

All other tissues were harvested, formalin-fixed, and paraffin-embedded for H&E staining.

hsRL Cytokine and Calcium Level Evaluation

The concentration of hsRL in the culture medium of transduced and untransduced HEK293T cells and of 2D or 3D cultured MSC was determined using the human sRANKL (total) Enzyme Linked Immunosorbent Assay (ELISA) kit (PromoCell GmbH, Heidelberg, Germany). Serum total calcium levels were determined using a Ci16200 Architect Abbott instrument (Abbott Park, Green Oaks, IL).

Statistical Analysis

Statistical analysis was performed using Mann–Whitney test or *t* test when comparing two groups. One-way or Two-way Anova with Tukey's post-test were used for multiple comparisons (GraphPad Prism 5.0, GraphPad Softwares Inc. La Jolla, CA). Statistical significance was considered when $p < .05$ ($^{*}p < .05$, $^{**}p < .01$, $^{***}p < .001$). All the experiments were performed at least in triplicate. All data are presented as mean $\pm$ SEM.

RESULTS

Validation of a Lentiviral Vector Expressing Human Soluble RANKL

We recently produced a third generation bidirectional lentiviral vector, expressing human soluble RANKL (LVhsRL), under the minimal core element of the CMV promoter (mhCMV) and the green fluorescent protein (GFP) under the human PGK (hPGK) promoter (Fig. 1A); the vector expressing only the GFP was used as a control [13]. We utilized the HEK293T cell line as commonly accepted for validation procedures [18, 26]. Namely, we transduced HEK293T cells with increasing amount of lentiviral particles, from 1 to 100 MOI for both the LVhsRL and mock vector. In both conditions, the fraction of transduced cells was directly proportional to the used MOI up to MOI 20, and no significant difference was found between MOI 20, 50 and 100, as assessed through GFP fluorescence by cytofluorimetric analysis (Fig. 1B, left plot); so the transduction efficiency of the two vectors was comparable. Mean Fluorescence Intensity (MFI) of GFP^+ cells was comparable at MOI 1–20, and higher at MOI 50 and 100 with both vectors (Fig. 1B, right plot), likely due to higher viral integration in these latter conditions. In addition, cell viability and growth, measured through the MTT test at 24, 48 and 72 hours posttransduction, inversely correlated to the used MOI, as expected (Fig. 1C). At all the time points, RANKL concentration was significantly higher in the supernatant of LVhsRL-transduced as compared to untransduced cells, as expected. In particular, in a short timeframe (within 3 days after transduction), no difference was observed between 1, 5, and 10 MOI. At 20, 50, and 100 MOI RANKL production significantly higher as compared to lower MOIs at all the time points. At 48 and 72 hours after transduction, cytokine levels were greatly reduced at MOI 50 and 100 (Fig. 1D), likely due to decreased cell viability at these MOIs; no such effect was observed at MOI 20. Then, we selected the conditions 10, 20, and 50 MOI for long-term culture (up to 12 days after transduction). In this period, cells of all experimental settings recovered as inferred by measuring RANKL production, which was sustained and proportional to the used MOI, as assessed both in the cells by Western blot and in the supernatant by ELISA assay (Fig. 1E). The achieved VCN was similar between LVhsRL-transduced and mock-transduced cells, with values of 4.56, 8.45, and 16.16 for cells transduced with the LVhsRL vector at 10, 20, and 50 MOI, and 3.02, 4.74, and 16.58 for cells transduced with the mock vector at the same MOIs.

Overall, these results showed that the LVhsRL vector was able to transduce effectively HEK293T cells and to achieve sustained soluble RANKL production. In addition, based on these data and foreseeing the usage of transduced cells shortly after transduction, we reasoned that 20 MOI provided an optimal balance between cell viability and RANKL production; therefore, the following experiments were performed at this MOI.

Functional Evaluation of the RANKL Cytokine Produced by Transduced HEK293T Cells

To assess whether the RANKL cytokine expressed by the lentiviral vector was biologically active, we verified whether it was capable of inducing osteoclast differentiation from mouse and human precursor cells; in fact, human RANKL is known to be effective on precursors from both species [27, 28]. In detail, the conditioned media (CM) of LVhsRL-transduced HEK293T cells (MOI 20) was used in a standard osteoclastogenesis assay in place of the recombinant RANKL cytokine; the CM of mock-transduced HEK293T cells was used in parallel, as a negative control. In this regard, it is worth mentioning here that the RANKL concentration in LVhsRL-transduced HEK293T supernatants was lower than that used in standard osteoclastogenesis protocols (i.e., 37.13 $\pm$ 0.8 pg/ml as compared to 20–100 ng/ml [29, 30]). Therefore, the CM from both LVhsRL-transduced and mock-transduced cells was concentrated by a factor of 50, achieving an hsRL concentration of 2.32 $\pm$ 0.28 ng/ml in the LVhsRL-CM, prior to application to the osteoclastogenesis assay.

Then, WT or $Rankl^{-/-}$ murine splenocytes and human peripheral blood mononuclear cells (PBMCs) from a healthy donor were cultured either on plastic or dentin discs in the presence of M-CSF and with or without the concentrated CM. At the end of the differentiation protocol, in the presence of RANKL-containing CM, osteoclasts formed from both murine and human precursor cells and resorbed dentin, as demonstrated by TRAP and toluidine blue staining, respectively. On the other hand, no differentiation was achieved in the presence of the concentrated mock CM (Fig. 2). The most obvious explanation to this result was that hsRL present in the LVhsRL CM endowed this supernatant with a pro-osteoclastogenic capacity.

Overall, these data confirmed that the RANKL cytokine expressed by the lentiviral vector was functional in vitro.

Production of a 3D Biomimetic Scaffold

We recently reported on the generation and characterization of murine bone marrow-derived WT and $Rankl^{-/-}$ MSCs, and the transduction of these latter with LVhsRL and mock lentiviral vectors [13]. In the framework of the present study, to favor MSC survival and proliferation, and enhance their functional

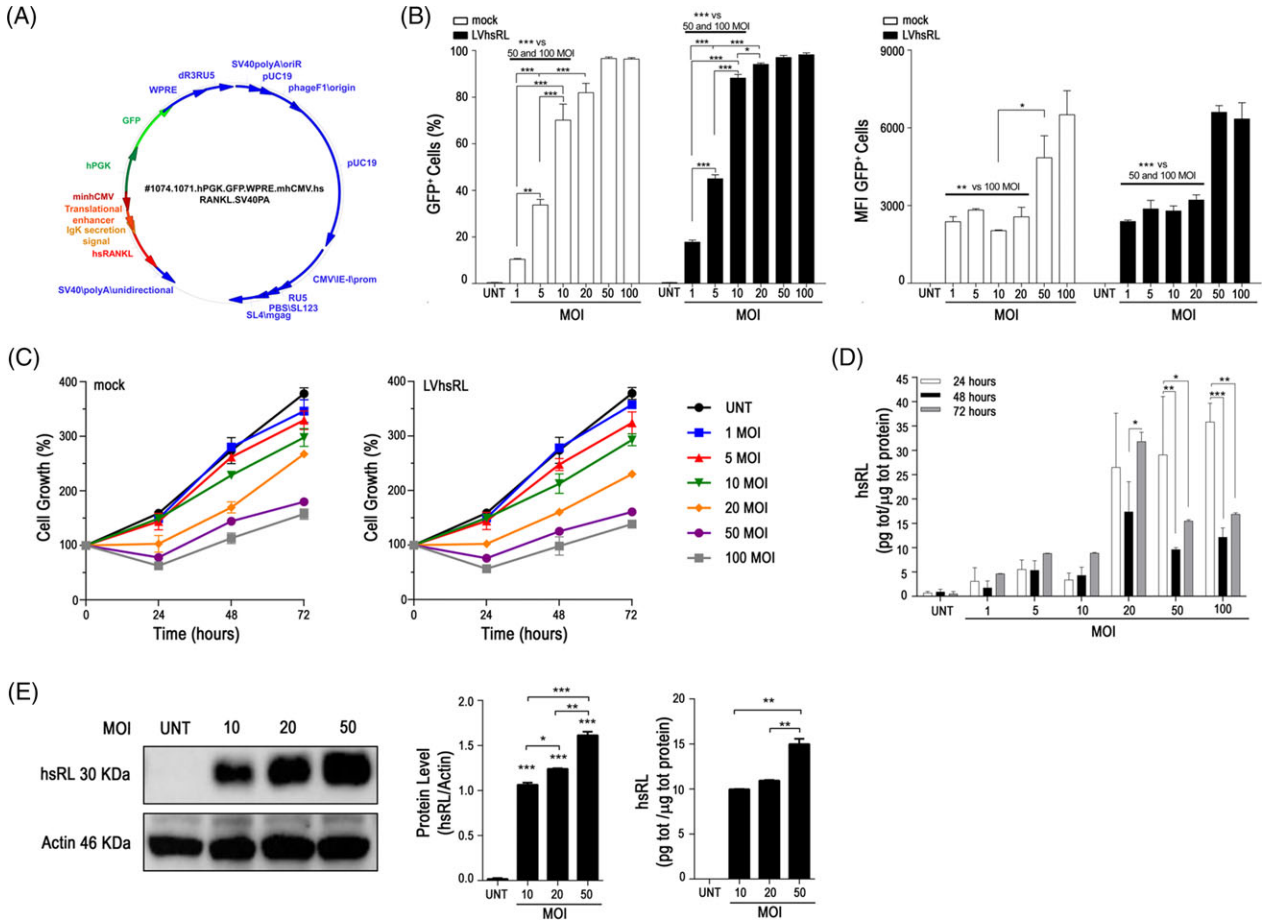

Figure 1. Validation of a lentiviral vector expressing human soluble RANKL (hsRL). **(A)** Schematic representation of the lentiviral vector for the expression of hsRL. **(B)** Quantization of HEK293T cell transduction with the LVhsRL and mock vector at increasing MOI, expressed as percentage of GFP^+ cells (left) and as GFP mean fluorescence intensity (MFI; right). **(C)** Evaluation of cell growth rate over time of untransduced and transduced HEK293T cells, by MTT assay. **(D)** Quantization of hsRL production over time by untransduced and transduced HEK293T cells, by ELISA assay on the corresponding supernatants. Only statistics between different time points of the same MOI is indicated. **(E)** Quantization of hsRL in protein extracts (left) and in supernatants (right) of untransduced and transduced HEK293T cells 2 weeks after transduction. $^{*}p < .05$; $^{**}p < .01$, $^{***}p < .001$.

properties, we set up a 3D culture. In detail, we generated a scaffold made of Magnesium-doped hydroxyapatite/collagen I (MgHA/Col), which could ideally mimic the physicochemical characteristics of the bone. The 3D hybrid composites were synthetized through a biomineralization process allowing nucleation of biomimetic HA nanoparticles on type I collagen fibers during their self-assembly guided by pH changes. SEM analysis showed the porosity and the whole hybrid's structure at low magnifications, and the formation of nanostructured and homogeneously distributed apatite nanocrystals aligned on collagen fibers, at high magnification (Fig. 3A). The assessment of the porosity of the hybrid composite with two different methods highlighted a total porosity close to 95% comprising nanopores and micropores and about 60% of macropores suitable for cell proliferation (Fig. 3B). TGA analysis revealed a weight ratio of the MgHA/Col hybrid composite 60/40 (Fig. 3C), so very close to the composition of the natural bone tissue [31]. FTIR spectra of the hybrid composite MgHA/Col and of an hydroxyapatite (HA) synthetized in the same condition and selected as reference material, revealed the presence of typical peaks of collagen together with those of apatite in the biomineralized material. In detail, the peaks at about 1,000 cm^{-1} and 600 cm^{-1} correspond to the apatite, while those between 1,300 cm^{-1} and 1,650 cm^{-1} correspond to the alpha-helical structure of collagen at amide I, II, and III. In particular, the shift from 1,340 cm^{-1} to 1,337 cm^{-1} was because of the stretching of COO^- groups of collagen, indicating the active interaction of collagen functional groups with the positively charged apatite crystals (Fig. 3D).

XRD analysis of the hybrid MgHA/Col and of the reference HA showed the typical peaks of low crystalline apatites; however, the mineral phase synthetized through the biomineralization process produced wider peaks. This indicated that the presence of Mg^{2+} ions and the template and structural confinement action of collagen fibers led to the formation of a less crystalline and thus more biomimetic mineral phase (Fig. 3E).

ICP analysis confirmed the presence of Magnesium in the final composite with evidence of a partial substitution of Calcium with Magnesium in the apatite lattice. In particular, ICP showed that about 70 wt.% of the initial nominal concentration of Mg^{2+} ions substituted Ca^{2+} in the apatite lattice, and that the Ca/P ratio of the MgHA nucleated on collagen was in the typical range of low crystalline apatite (1.45–1.60), as expected (Fig. 3B). Finally, this material had high hydrophilicity and very low-degradation rate, thanks to the stability

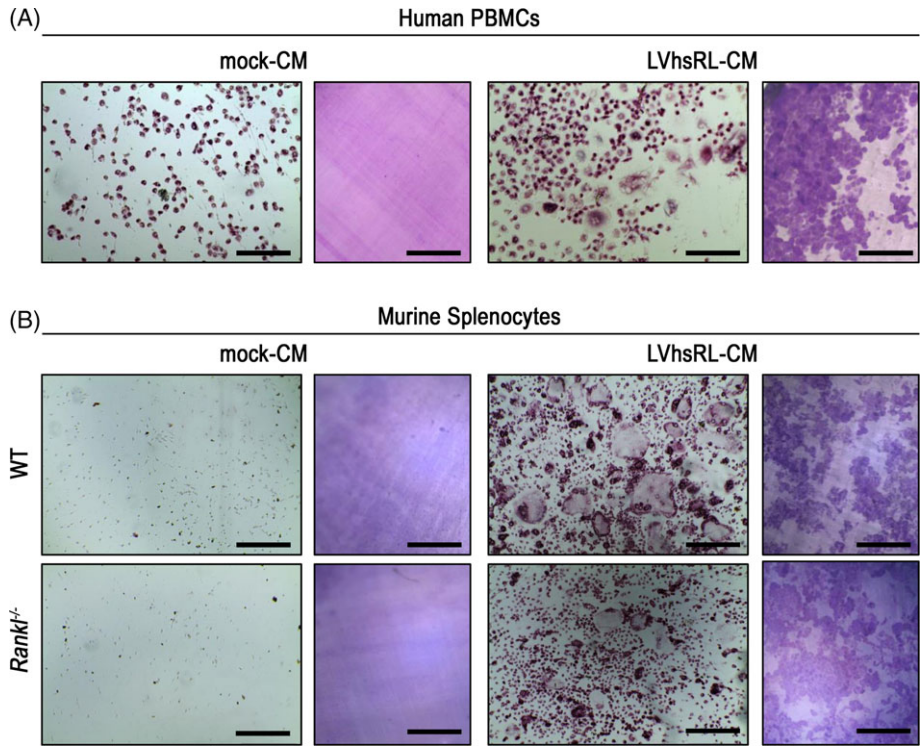

Figure 2. Functional evaluation of hsRL produced by transduced HEK293T cells. Osteoclastogenesis and resorption assays from **(A)** human PBMCs and **(B)** murine WT and *Rankl*$^{-/-}$ splenocytes in the presence of M-CSF and ×50 concentrated conditioned medium from mock-transduced and LVhsRL-transduced HEK293T cells (left and right plots, respectively). Mature osteoclasts were identified by TRAP staining, while resorption pits were visualized by staining dentin discs with toluidine blue. Scale bars: 200 μm **(A)**; 400 μm **(B)**.

conferred by the crosslinking action of BDDGE [20] (Fig. 3F, 3G). Overall, these properties made our scaffold particularly suited for in vitro and in vivo experiments.

MSC Culture on MgHA/Col Scaffolds

As above explained, our strategy is based on the use of MSC. Thus, we exploited WT and *Rankl*$^{-/-}$ MSC lines previously generated and afterward transduced at MOI 20 according to the validation experiments [13]. For the present purpose, we first studied MSC behavior on the produced scaffolds in terms of cell morphology and interactions, attachment to the collagen fibers and invasion. To this end, we took advantage of GFP expression by transduced MSCs, on one hand, and of collagen autofluorescence, on the other. Initially, cells appeared to distribute on top of the scaffold, showing their typical "fibroblast-like" shape, to organize and firmly attach along the collagen fibers. As early as 48 hours after seeding, they had entered the scaffold and begun to colonize it; in addition, cell proliferation and cell-to-cell contacts appeared to increase over time. On the other hand, the scaffold itself was modified and remodeled over time by the invading cells (Fig. 4A).

Then, we compared cell proliferation in 2D versus 3D culture on the produced scaffold. At all time points, cell growth, determined as fold increase as compared to day 0, was greater in 3D than in 2D cultures, irrespective of the genotype, or vector used for transduction (Fig. 4B and Supporting Information Table S1). Furthermore, the amount of cytokine produced by the LVhsRL-transduced cells upon 3D culture was significantly higher as compared to the 2D setting (Fig. 4C); in contrast, the RANKL cytokine was absent in mock-transduced *Rankl*$^{-/-}$ MSCs culture medium, as expected ([13] and data not shown).

Overall, these data demonstrated that our MgHA/Col scaffold was a good substrate for MSCs culture: seeded cells adhered nicely and interacted with the provided support and extensively colonized it; moreover, their viability was maintained and proliferation was increased over time. Thus, the cytokine production was significantly enhanced.

In Vivo Implantation

We already reported evidence showing that a similar cell-scaffold construct was well tolerated and osteoinductive in immunodeficient mice [13]. Here, we verified the in vivo biocompatibility of the cell-seeded MgHA/Col scaffold and the effect of lentivirally mediated RANKL production in the *Rankl*$^{-/-}$ mouse. In detail, *Rankl*$^{-/-}$ mice underwent subcutaneous implantation of a scaffold seeded with 7×10^5 cells, which were either LVhsRL-transduced or mock-transduced *Rankl*$^{-/-}$ MSCs or WT MSCs, as controls; the seeding efficiency was about 90%. After surgery, the animals were monitored for 2 months; in this timeframe, no sign of distress was apparent. At necropsy, the scaffold, long bones, spine, and selected tissues were harvested and processed for histological analysis. Hematoxilin-Eosin (H&E) staining of the scaffolds showed that, irrespectively of the specific type of seeded cells, they were well colonized by live cells and extensively vascularized; the presence of vessels was confirmed by immunostaining for CD31 (Fig. 5A, left plots). This evidence supports the hypothesis that soluble factors produced by the implanted MSCs, also comprising the RANKL cytokine, could reach the general circulation, thus possibly eliciting a biological effect. Of note, the cells populating the scaffolds were at least in part of donor origin, as demonstrated by GFP positive immunohistochemical staining in scaffolds initially seeded with transduced cells (Fig. 5B, left plots);

(A)

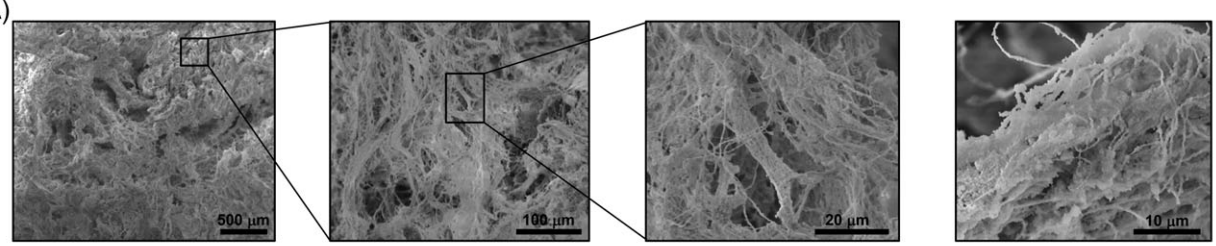

(B)

Porosity MgHA/Col		ICP Analysis		
			MgHA/Col molar ratio	Stoichiometric HA powder (Mg, CO_3 apatite)
Density Method	95±1%			
Water Squeezing Method	61±4%	Ca/P	1.54±0.01	1.67
Density (g/cm^3)	0.13±0.03	Mg/Ca (%)	3.3±0.1	-
		(Ca + Mg)/P	1.59±0.01	-

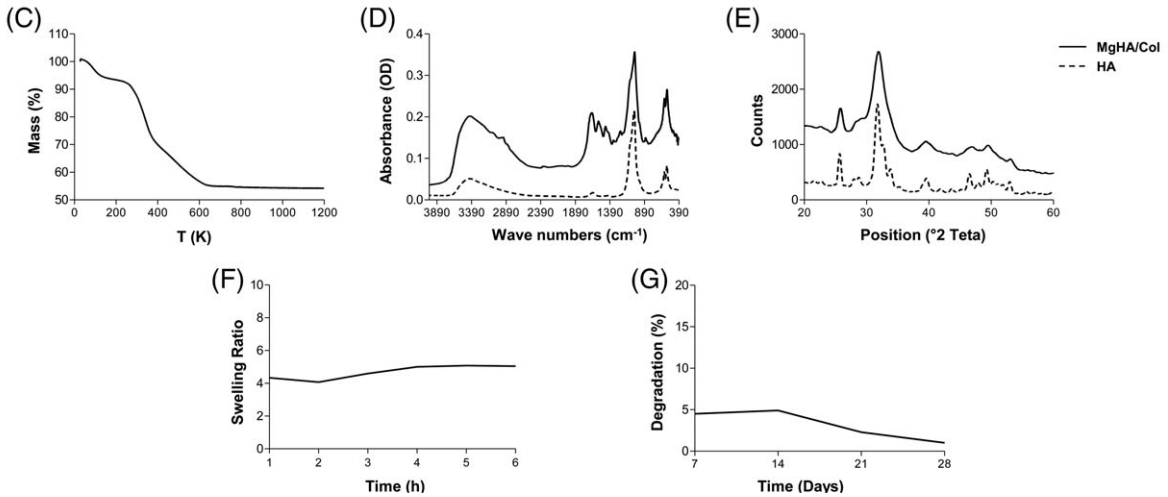

Figure 3. Characterization of 3D biomimetic MgHA/Col scaffold. **(A)** Scanning Electron Microscopy micrographs at different magnifications, showing scaffold porosity and micro-architectures of the hybrid composite. **(B)** Porosity and chemical composition of the hybrid MgHA/Col scaffold. **(C)** TGA, **(D)** FTIR, and **(E)** XRD analysis. In plots D and E, the solid line indicates the MgHA/Col, while the dashed one the HA. **(F)** Evaluation of the swelling ratio and **(G)** percentage of degradation of MgHA/Col scaffolds overtime.

it could be reasonably inferred, even though we have not formally proven, that the same will have occurred in WT MSC-seeded scaffolds. In addition, a large number of cells found on the scaffolds were represented by $F4/80^+$ macrophages from the host (Supporting Information Fig. S1).

Next, we assessed whether the implanted cell-scaffold constructs affected the skeletal phenotype of *Rankl*$^{-/-}$ mice. TRAP staining revealed the presence of $TRAP^+$ cells specifically in the bone of *Rankl*$^{-/-}$ mice implanted with a WT or LVhsRL-transduced *Rankl*$^{-/-}$ MSC-seeded scaffold, while no $TRAP^+$ cells were found in *Rankl*$^{-/-}$ mice implanted with a mock-transduced *Rankl*$^{-/-}$ MSC-seeded scaffold (Fig. 6A, left plots, and 6B), in accordance with previous reports on the absence of $TRAP^+$ cells in the *Rankl*$^{-/-}$ mouse model [9]. This suggests that the hsRL molecule secreted by WT and LVhsRL-transduced *Rankl*$^{-/-}$ MSCs can induce to a certain extent formation of $TRAP^+$ cells, which could be reasonably regarded as cells of the osteoclast lineage.

To enhance the effect at the cellular level, we performed another group of experiments, in which 1.5×10^6 cells where seeded on each scaffold, with a seeding efficiency of about 80%, and 2 scaffolds were implanted in each *Rankl*$^{-/-}$ mouse; after sacrifice we carried out the same evaluations as above. Histological analysis of the harvested cell-scaffold constructs showed abundant vascularization and a more prominent presence of cells, comprising also of GFP^+ ones, as expected based on the higher number of cells initially seeded (Fig. 5, right plots). Within the bone tissue, we found a clear increase in $TRAP^+$ cells in the bone of *Rankl*$^{-/-}$ mice implanted with WT MSC-seeded scaffolds and even more in those implanted with LVhsRL-transduced *Rankl*$^{-/-}$ MSC-seeded scaffolds, as compared with mice of the same treatment group with a single scaffold. On the other hand, $TRAP^+$ cells were still completely absent in the control group (i.e., *Rankl*$^{-/-}$ mice plus mock-transduced *Rankl*$^{-/-}$ MSC-seeded scaffolds), as expected (Fig. 6A, right plots, and 6B). Serological analysis of

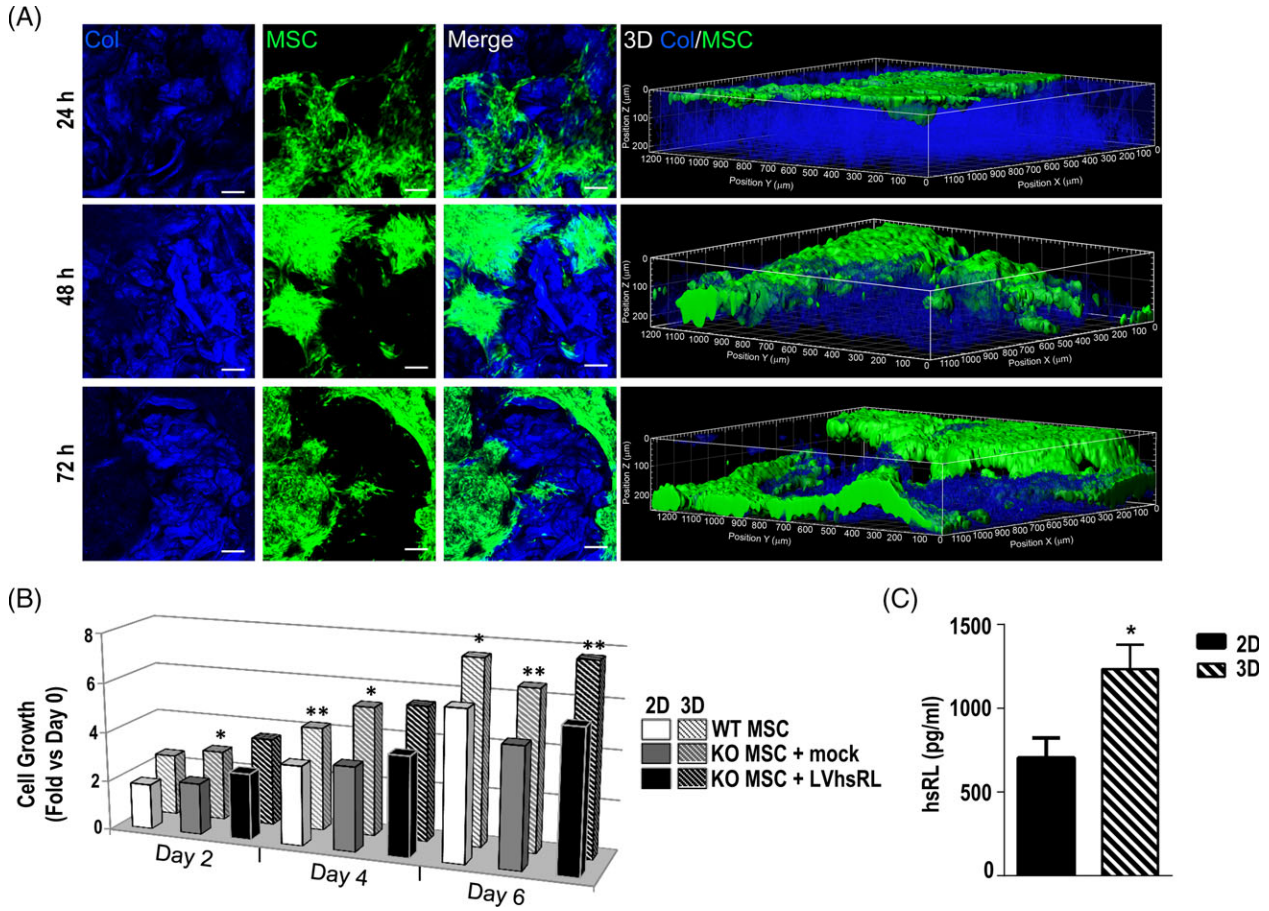

Figure 4. Characterization of MSC culture on MgHA/Col scaffolds. **(A)** Confocal analysis of LVhsRL-transduced *Rankl*$^{-/-}$ MSC-seeded scaffolds at different time points; blue color corresponds to collagen fibers, green to MSCs. Scale bar: 200 μm **(B)** Assessment of WT, mock-transduced and LVhsRL-transduced *Rankl*$^{-/-}$ MSC proliferation in 2D versus 3D culture overtime by MTT assay. Cell growth is expressed as fold increase compared to time 0. Statistics is referred to comparison of 2D versus 3D for each group. Cell growth fold increase data ± SEM are reported in Supporting Information Table 1. **(C)** Evaluation of hsRL concentration in the supernatant of LVhsRL-transduced *Rankl*$^{-/-}$ MSCs in 2D versus 3D culture by ELISA assay. $^{*}p < .05$; $^{**}p < .01$.

bone-related parameters showed a significant increase of total calcium in mice implanted with WT-transduced and LVhsRL-transduced *Rankl*$^{-/-}$ MSC-seeded scaffolds, even though physiological levels were not reached (Fig. 6C). Nonetheless, independent of the type of implanted construct, the classic osteopetrotic features were still present in the treated *Rankl*$^{-/-}$ mice, as shown by H&E staining: bone was very dense, with cartilage remnants, and no clear evidence of remodeling and very few marrow cells (Fig. 7). Accordingly, no difference was found in serum TRAP activity among the groups (data not shown).

We also evaluated whether the in vivo implantation of these constructs, and in particular the continuous release of hsRL by LVhsRL-transduced cells, caused any side effect. At sacrifice, no gross abnormality potentially related to the performed procedure was observed, nor were pathological signs found by standard histological analysis of selected organs, including liver, kidney, and lung (Supporting Information Fig. S2).

Discussion

The combination of biomaterials mimicking bone extracellular matrix and MSCs or engineered MSCs is a valid option for regenerative medicine and for cell-based tissue engineering therapies [32].

In particular, MSCs might serve as long-lasting reservoir of biologically active compounds [33, 34].

Accordingly, here we used a biocompatible hybrid scaffold composed of type I collagen and Magnesium-doped HA, seeded with either murine WT or *Rankl*$^{-/-}$ MSCs-transduced with a lentiviral vector restoring RANKL production, and implanted in *Rankl*$^{-/-}$ mice, to provide mice the missing essential osteoclastogenic factor. A scaffold with the same composition had been already used and reported to support in vivo MSC osteogenic differentiation [13, 35]. In the present work, this composite was produced through an ad hoc modified procedure that allowed achieving features of natural bone on the mandatorily reduced scale (i.e., the same size as the well of a 96-well plate) required by the small size of *Rankl*$^{-/-}$ mice [9]. Cross-linked collagen type I fibrils, the main component of the osteoid in vivo, served as templates onto which the inorganic elements settled, thus forming a mineralized bone matrix. The presence of Mg^{2+} ions inside the nucleated HA lattice and the chemical interaction between the mineral and the organic phase constrained the nucleation of apatite and reduced its crystallinity. These features made the obtained hybrid highly biomimetic, especially with respect toyoung and immature bone, and favored its biological properties. In fact, previous studies [2, 13, 35] and the present work demonstrated that this kind of scaffold

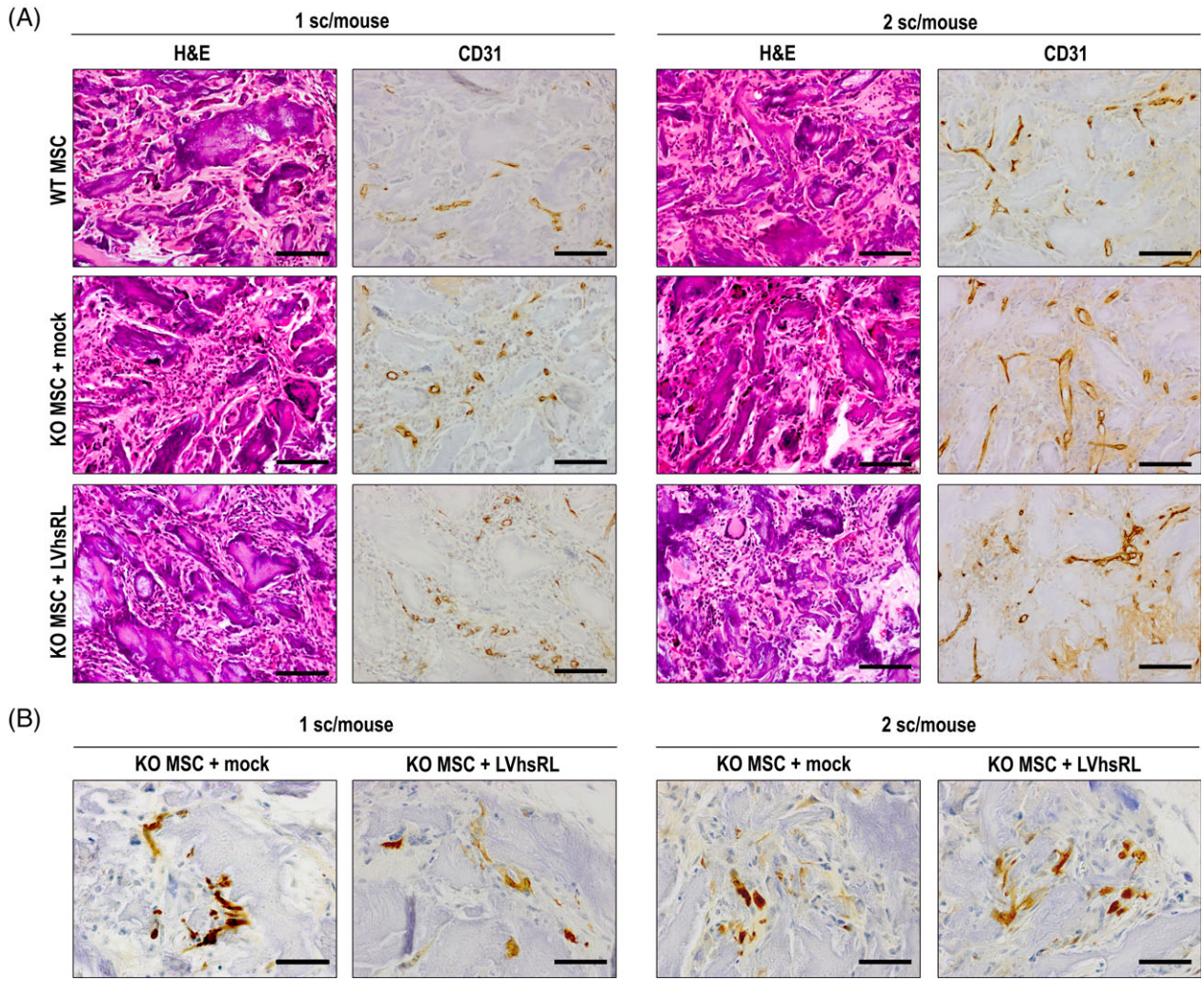

Figure 5. Histological analysis of MSC-seeded MgHA/Col scaffolds after 2 months implantation in *Rankl*$^{-/-}$ mice. **(A)** Hematoxylin–Eosin staining and CD31 immunostaining on serial sections of decalcified scaffolds from the different groups of treatment. Scale bar: 100 μm. **(B)** GFP immunostaining on sections of decalcified scaffolds from the different groups of treatment. Scale bar: 50 μm.

was bioactive, biodegradable, biocompatible, and easily recognized by cells, thanks to the high hydrophilicity and porosity, particularly in terms of macropores, which fostered cell adhesion, colonization, proliferation, and RANKL cytokine production, in agreement with reports in literature referring to different contexts [36, 37]. Moreover, once implanted subcutaneously in mice, these scaffolds were extensively vascularized; in line with other findings [38, 39], this should have favored graft-host interaction and MSCs survival, and supported the systemic distribution of soluble factors, likely comprising also RANKL, produced by the implanted cells.

Another strength of our approach is the optimization of murine MSC transduction with a lentiviral vector establishing continuous production of human soluble RANKL [13], which promoted osteoclastogenesis in vitro. Implantation of cell-seeded scaffolds in *Rankl*$^{-/-}$ mice led to TRAP^{+} cells formation in knock-out mice receiving the implant of a single LVhsRL-producing cell construct, indicating that the released cytokine was functional in vivo, too. In parallel, a similar result was not observed either in vitro or in vivo in the presence of mock-transduced *Rankl*$^{-/-}$ MSCs, further proving that the biological response elicited was dependent on the RANKL molecule expressed by the viral vector. We could not formally demonstrate the presence of hsRL in the sera of *Rankl*$^{-/-}$ mice implanted with LVhsRL-expressing constructs, but this was not surprising, as in other experimental settings a short half-life of exogenous RANKL in the circulation has been reported [9, 27].

No major side effect of these implants was observed over the 2 month follow-up period or at necropsy, indicating that this treatment was safe. On the other hand, the biological effect attained in *Rankl*$^{-/-}$ mice was limited and no amelioration of the osteopetrotic phenotype was observed. These results prompted us to conceive a strategy that could possibly enhance the benefit gained on the skeletal tissue of *Rankl*$^{-/-}$ mice by increasing the amount of cytokine delivered in vivo. To reach this goal, we increased the number of cells seeded on each scaffold and the number of cell constructs implanted in each mouse, even though no more than two of them could be inserted in the subcutaneous pouch on the back of *Rankl*$^{-/-}$ mice because of their severe growth retardation [9]. These changes to the protocol led to an increase in TRAP^{+} cell formation in the bones of *Rankl*$^{-/-}$ mice receiving RANKL-producing cell constructs, but again the skeletal defect was not improved. Thus, at present the pharmacological administration of soluble

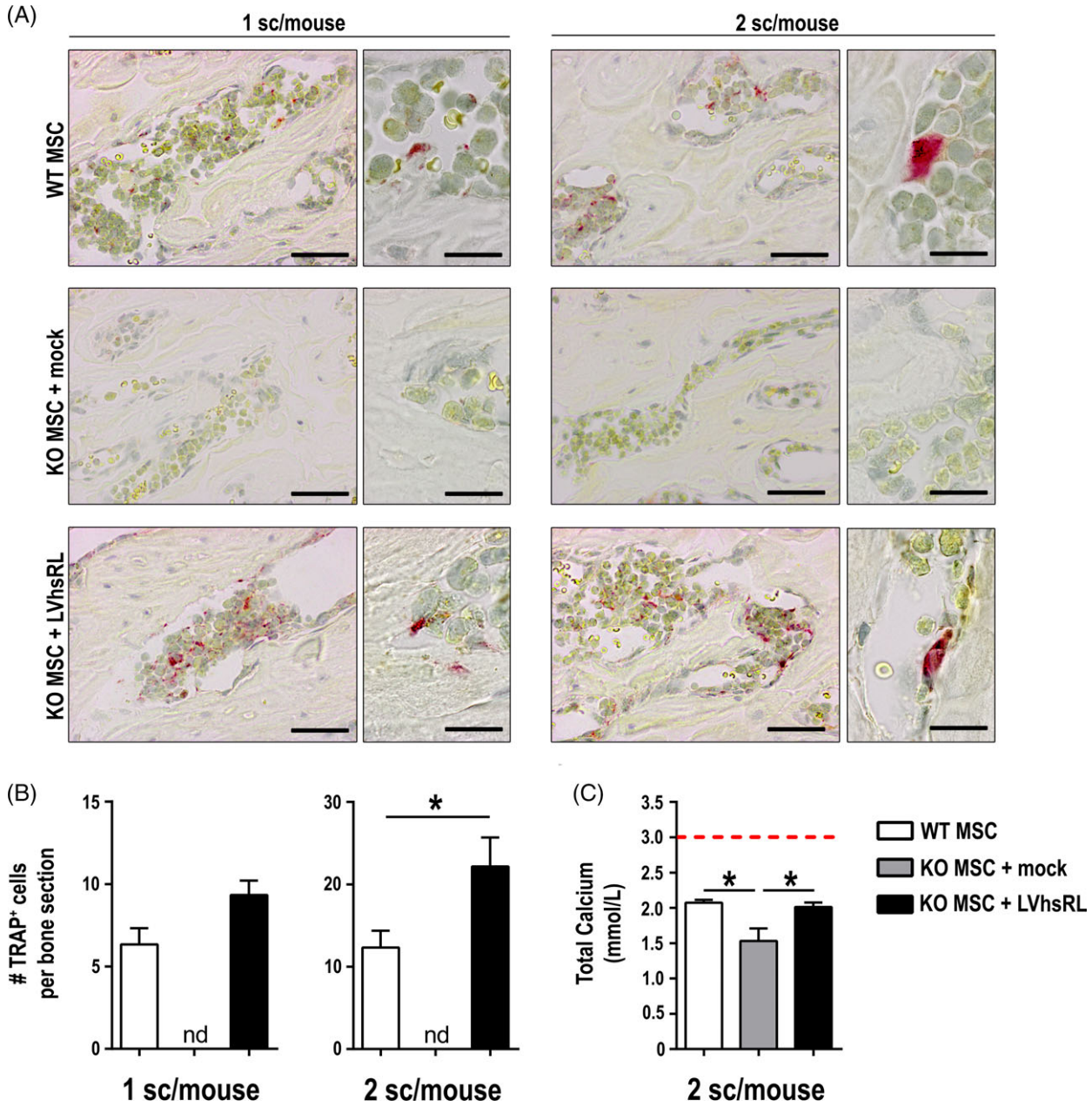

Figure 6. Evaluation of the effect of cell-constructs implantation on the bone phenotype of *Rankl*$^{-/-}$ mice. **(A)** TRAP staining on long bone of *Rankl*$^{-/-}$ mice belonging to the different treatment groups. Scale bars: 50 μm (left); 20 μm (right). **(B)** Number of TRAP^{+} cells per bone section of treated *Rankl*$^{-/-}$ mice. nd: not detected. **(C)** Measurement of serum total calcium concentration in treated *Rankl*$^{-/-}$ mice. The red dashed line indicates the average concentration in age matched wild type mice. $^{*}p < .05$.

RANKL appears to be the most effective treatment for RANKL ARO [9, 10]. Possible reasons for the failure of the approach herein described to correct the ARO-phenotype of *Rankl*$^{-/-}$ mice could be the limited amount of cytokine produced by WT and LVhsRL-transduced *Rankl*$^{-/-}$ MSCs [13]; in the latter case, this was dependent on the used MOI. Another possible explanation could be the extensive colonization of the scaffold by immune cells of the host, in particular a high number of macrophages, which might have eliminated a significant fraction of the cells originally seeded [40]. More substantial modifications of the protocol, than those used in the present study, would be necessary to improve the outcome of this approach. For example, we might consider increasing hsRL production by transduced cells, by using a higher MOI; using telomerase overexpression in LVhsRL-transduced *Rankl*$^{-/-}$ MSCs to augment their proliferation [41]; implanting a higher number of scaffolds or larger scaffolds (as far as this is technically feasible in these small mice); using a biomimetic smart scaffold functionalized to enhance MSC attachment [42]; isolating the system from the host cells by means of newly developed cell encapsulation systems, thus preventing its disruption [43]. The optimization of these aspects might be pursued, for example, by exploiting the emerging technology of rechargeable devices containing 3D printed cell-seeded functionalized scaffolds [44], which has already achieved promising results in other fields. Thus, the integration of the strengths of our strategy with these new tools will likely achieve a net improvement.

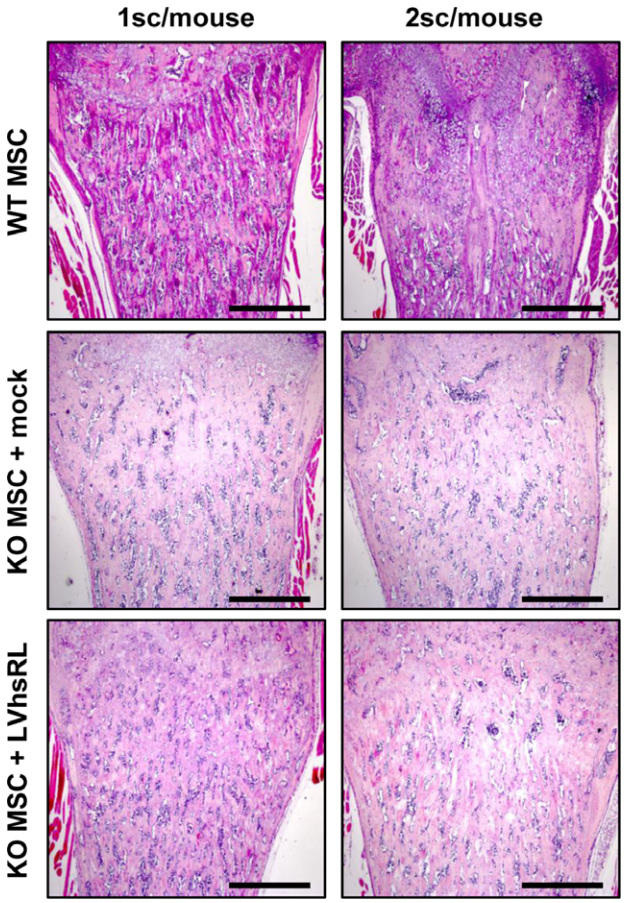

Figure 7. Histological analysis of bone after 2 months MSC-seeded MgHA/Col scaffolds implantation in *Rankl*$^{-/-}$ mice. H&E staining on sections of decalcified femurs from the different groups of treatment. Scale bar: 500 μm.

Conclusion

In this work, we have utilized a lentiviral vector for the stable expression of hsRL, which sustained in vitro human and mouse osteoclast differentiation. We have transduced *Rankl*$^{-/-}$ MSCs and set up conditions for their 3D culture on an MgHA/Col biomimetic scaffold. In particular, the chemical and physical properties of this scaffold enhanced MSC proliferation and hsRL production. After implantation of these MSC-seeded constructs in *Rankl*$^{-/-}$ mice, TRAP^{+} cells formed in bone, thus providing proof of principle of the capacity of this approach to support cell differentiation towards the osteoclast lineage in vivo. Optimization of the experimental setting exploiting also the most recent biotechnological tools will increase the efficacy of this strategy on the bone compartment. As a perspective, we might pursue further implementation of this system using patients-derived cells for a future possible autologous cell and gene therapy approach.

Acknowledgments

We thank Dario Strina and Sonia Valentino for technical support. This work was partially supported by the European Community's Seventh Framework Program (FP7/2007-2013, SYBIL Project) and PRIN Project (2015F3JHMB_004) to AV, and by Programma Nazionale per la Ricerca-Consiglio Nazionale delle Ricerche Aging Project to AV. AI is recipient of a Young Investigator Grant from Ministero della Salute (GR-2011-02349539). CM is recipient of a fellowship founded by Fondazione Nicola Del Roscio.

Author Contributions

C.M.: Conception and design, data collection and analysis, manuscript writing, and final approval; E.C.: Data collection and analysis, final approval of manuscript; E.P.: Data collection, final approval of manuscript.; S.M.: Data collection, final approval of manuscript; M.E.: Data collection and analysis, final approval of manuscript; A.I.: Data collection and analysis, final approval of manuscript; E.F.: Data analysis, final approval of manuscript; F.S.: Provision of study material, final approval of manuscript; R.v.H.: Data collection, final approval of manuscript; M.S.: Provision of study material, data collection and analysis, manuscript writing and final approval; A.T.: Provision of study material, final approval of manuscript; A.V.: Conception and design, financial support, final approval of manuscript; C.S.: Conception and design, data interpretation, manuscript writing, and final approval.

Disclosure of Potential Conflicts of Interest

All the authors declare nothing to disclose.

References

1 Rebelo MA, Alves TF, de Lima R et al. *Scaffolds and tissue regeneration: An overview of the functional properties of selected organic tissues*. J Biomed Mater Res B Appl Biomater 2016;104(7):1483-1494. https://doi.org/10.1002/jbm.b.33482.

2 Scaglione S, Giannoni P, Bianchini P et al. *Order versus Disorder: in vivo bone formation within osteoconductive scaffolds*. Sci Rep 2012;2:274. https://doi.org/10.1038/srep00274.

3 Li, J.J., M. Ebied, J. Xu, and H. Zreiqat, *Current Approaches to Bone Tissue Engineering: The Interface between Biology and Engineering.* Adv Healthc Mater, 2017.https://doi.org/10.1002/adhm.201701061

4 Fernandez-Yague MA, Abbah SA, McNamara L et al. *Biomimetic approaches in bone tissue engineering: Integrating biological and physicomechanical strategies*. Adv Drug Deliv Rev 2015;84:1-29. https://doi.org/10.1016/j.addr.2014.09.005.

5 Mravic M, Peault B, James AW. *Current trends in bone tissue engineering*. Biomed Res Int 2014;2014:865270. https://doi.org/10.1155/2014/865270.

6 Sobacchi C, Schulz A, Coxon FP et al. *Osteopetrosis: genetics, treatment and new insights into osteoclast function*. Nat Rev Endocrinol 2013;9(9):522-536. https://doi.org/10.1038/nrendo.2013.137.

7 Sobacchi C, Frattini A, Guerrini MM et al. *Osteoclast-poor human osteopetrosis due to mutations in the gene encoding RANKL*. Nat Genet 2007;39(8):960-962. https://doi.org/10.1038/ng2076.

8 Lo Iacono N, Pangrazio A, Abinun M et al. *RANKL cytokine: from pioneer of the osteoimmunology era to cure for a rare disease*. Clin Dev Immunol 2013;2013:412768. https://doi.org/10.1155/2013/412768.

9 Lo Iacono N, Blair HC, Poliani PL et al. *Osteopetrosis rescue upon RANKL administration to Rankl(−/−) mice: a new therapy for human RANKL-dependent ARO*. J Bone Miner Res 2012;27(12):2501-2510. https://doi.org/10.1002/jbmr.1712.

10 Cappariello A, Paone R, Maurizi A et al. *Biotechnological approach for systemic delivery of membrane Receptor Activator of*

NF-kappaB Ligand (RANKL) active domain into the circulation. Biomaterials 2015;46: 58-69. https://doi.org/10.1016/j.biomaterials.2014.12.033.

11 Sobacchi C, Palagano E, Villa A et al. *Soluble Factors on Stage to Direct Mesenchymal Stem Cells Fate*. Front Bioeng Biotechnol 2017;5:32. https://doi.org/10.3389/fbioe.2017.00032.

12 Murphy MB, Moncivais K, Caplan AI. *Mesenchymal stem cells: environmentally responsive therapeutics for regenerative medicine*. Exp Mol Med 2013;45:e54. https://doi.org/10.1038/emm.2013.94.

13 Schena F, Menale C, Caci E et al. *Murine Rankl–/– Mesenchymal Stromal Cells Display an Osteogenic Differentiation Defect Improved by a RANKL-Expressing Lentiviral Vector.* Stem Cells 2017;35(5):1365-1377. https://doi.org/10.1002/stem.2574.

14 Nakashima T, Hayashi M, Fukunaga T et al. *Evidence for osteocyte regulation of bone homeostasis through RANKL expression*. Nat Med 2011;17(10):1231-1234. https://doi.org/10.1038/nm.2452.

15 Xiong J, Onal M, Jilka RL et al. *Matrix-embedded cells control osteoclast formation*. Nat Med 2011;17(10):1235-1241. https://doi.org/10.1038/nm.2448.

16 Oggu GS, Sasikumar S, Reddy N et al. *Gene Delivery Approaches for Mesenchymal Stem Cell Therapy: Strategies to Increase Efficiency and Specificity.* Stem Cell Review 2017;13(6):725-740. https://doi.org/10.1007/s12015-017-9760-2.

17 Yousefi AM, James PF, Akbarzadeh R et al. *Prospect of Stem Cells in Bone Tissue Engineering: A Review.* Stem Cells International 2016;2016:6180487. https://doi.org/10.1155/2016/6180487.

18 Annoni A, Cantore A, Della Valle P et al. *Liver gene therapy by lentiviral vectors reverses anti-factor IX pre-existing immunity in haemophilic mice*. EMBO Mol Med 2013; 5(11):1684-1697. https://doi.org/10.1002/emmm.201302857.

19 Roveri N, Falini G, Sidoti MC et al. Biologically inspired growth of hydroxyapatite nanocrystals inside self-assembled collagen fibers. Mater Sci Eng C-Biomimetic Supramole Syst 2003;23(3):441-446.

20 Krishnakumar GS, Gostynska N, Dapporto M et al. *Evaluation of different crosslinking agents on hybrid biomimetic collagen-hydroxyapatite composites for regenerative medicine*. Int J Biol Macromol 2018; 106:739-748. https://doi.org/10.1016/j.ijbiomac.2017.08.076.

21 Nicoletti A, Fiorini M, Paolillo J et al. Effects of different crosslinking conditions on the chemical-physical properties of a novel bio-inspired composite scaffold stabilised with 1,4-butanediol diglycidyl ether (BDDGE). J Mater Sci-Mater Med 2013;24(1):17-35.

22 Shankar KG, Gostynska N, Montesi M et al. Investigation of different cross-linking approaches on 3D gelatin scaffolds for tissue engineering application: A comparative analysis. Int J Biol Macromol 2017;95: 1199-1209.

23 Mao JS, Zhao LG, Yin YJ et al. Structure and properties of bilayer chitosan-gelatin scaffolds. Biomaterials 2003; 24(6):1067-1074.

24 Arora A, Kothari A, Katti DS. *Pore orientation mediated control of mechanical behavior of scaffolds and its application in cartilage-mimetic scaffold design*. J Mech Behav Biomed Mater 2015;51:169-183. https://doi.org/10.1016/j.jmbbm.2015.06.033.

25 Kim N, Odgren PR, Kim DK et al. *Diverse roles of the tumor necrosis factor family member TRANCE in skeletal physiology revealed by TRANCE deficiency and partial rescue by a lymphocyte-expressed TRANCE transgene*. Proc Natl Acad Sci U S A 2000;97(20): 10905-10910. https://doi.org/10.1073/pnas.200294797.

26 Sena-Esteves, M. and G. Gao, *Titration of Lentivirus Vectors*. Cold Spring Harb Protoc, 2018. 2018(4): p. pdb prot095695.https://doi.org/10.1101/pdb.prot095695

27 Tomimori Y, Mori K, Koide M et al. *Evaluation of pharmaceuticals with a novel 50-hour animal model of bone loss*. J Bone Miner Res 2009;24(7):1194-1205. https://doi.org/10.1359/jbmr.090217.

28 Lloyd SA, Yuan YY, Kostenuik PJ et al. *Soluble RANKL induces high bone turnover and decreases bone volume, density, and strength in mice*. Calcif Tissue Int 2008;82(5): 361-372. https://doi.org/10.1007/s00223-008-9133-6.

29 Neri T, Muggeo S, Paulis M et al. *Targeted Gene Correction in Osteopetrotic-Induced Pluripotent Stem Cells for the Generation of Functional Osteoclasts*. Stem Cell Reports 2015;5(4):558-568. https://doi.org/10.1016/j.stemcr.2015.08.005.

30 Marino S, Logan JG, Mellis D et al. *Generation and culture of osteoclasts*. Bonekey Rep 2014;3:570. https://doi.org/10.1038/bonekey.2014.65.

31 Gao C, Peng S, Feng P et al. *Bone biomaterials and interactions with stem cells*. Bone Res 2017;5:17059. https://doi.org/10.1038/boneres.2017.59.

32 Haj J, Haj Khalil T, Falah M et al. *An ECM-Mimicking, Mesenchymal Stem Cell-Embedded Hybrid Scaffold for Bone Regeneration*. Biomed Res Int 2017; 2017:8591073. https://doi.org/10.1155/2017/8591073.

33 Konala VB, Mamidi MK, Bhonde R et al. *The current landscape of the mesenchymal stromal cell secretome: A new paradigm for cell-free regeneration*. Cytotherapy 2016; 18(1):13-24. https://doi.org/10.1016/j.jcyt.2015.10.008.

34 Volarevic V, Gazdic M, Simovic Markovic B et al. *Mesenchymal stem cell-derived factors: Immuno-modulatory effects and therapeutic potential*. Biofactors 2017;43(5):633-644. https://doi.org/10.1002/biof.1374.

35 Minardi S, Corradetti B, Taraballi F et al. *Evaluation of the osteoinductive potential of a bio-inspired scaffold mimicking the osteogenic niche for bone augmentation*. Biomaterials 2015; 62:128-137. https://doi.org/10.1016/j.biomaterials.2015.05.011.

36 Su N, Gao PL, Wang K et al. *Fibrous scaffolds potentiate the paracrine function of mesenchymal stem cells: A new dimension in cell-material interaction*. Biomaterials 2017; 141:74-85. https://doi.org/10.1016/j.biomaterials.2017.06.028.

37 Rashedi I, Talele N, Wang XH et al. *Collagen scaffold enhances the regenerative properties of mesenchymal stromal cells*. PLoS One 2017;12(10):e0187348. https://doi.org/10.1371/journal.pone.0187348.

38 Calabrese G, Giuffrida R, Forte S et al. *Human adipose-derived mesenchymal stem cells seeded into a collagen-hydroxyapatite scaffold promote bone augmentation after implantation in the mouse*. Sci Rep 2017;7(1):7110. https://doi.org/10.1038/s41598-017-07672-0.

39 Gauthaman K, Fong CY, Venugopal JR et al. *Propagation and differentiation of human Wharton's jelly stem cells on three-dimensional nanofibrous scaffolds*. Methods Mol Biol 2013;1058:1-23. https://doi.org/10.1007/7651_2012_1.

40 Nair A, Tang L. *Influence of scaffold design on host immune and stem cell responses*. Semin Immunol 2017;29:62-71. https://doi.org/10.1016/j.smim.2017.03.001.

41 Simonsen JL, Rosada C, Serakinci N et al. *Telomerase expression extends the proliferative life-span and maintains the osteogenic potential of human bone marrow stromal cells*. Nat Biotechnol 2002;20(6):592-596. https://doi.org/10.1038/nbt0602-592.

42 Ramirez-Rodriguez GB, Montesi M, Panseri S et al. *(*) Biomineralized Recombinant Collagen-Based Scaffold Mimicking Native Bone Enhances Mesenchymal Stem Cell Interaction and Differentiation*. Tissue Eng Part A 2017;23(23–24): 1423-1435. https://doi.org/10.1089/ten.TEA.2017.0028.

43 Sabek, O.M., M. Farina, D.W. Fraga, S. Afshar, A. Ballerini, C.S. Filgueira, U. R. Thekkedath, A. Grattoni, and A.O. Gaber, Three-dimensional printed polymeric system to encapsulate human mesenchymal stem cells differentiated into islet-like insulin-producing aggregates for diabetes treatment. J Tissue Eng, 2016. 7: p. 2041731416638198. 10.1177/2041731416638198

44 Farina M, Ballerini A, Fraga DW et al. *3D Printed Vascularized Device for Subcutaneous Transplantation of Human Islets*. Biotechnol J 2017;12(9). https://doi.org/10.1002/biot.201700169.

See www.StemCellsTM.com for supporting information available online.